

Quantum Chaos Triggered by Precursors of a Quantum Phase Transition: The Dicke Model

Clive Emary* and Tobias Brandes

Department of Physics, UMIST, P.O. Box 88, Manchester M60 1QD, U. K.

(Dated: October 28, 2018)

We consider the Dicke Hamiltonian, a simple quantum–optical model which exhibits a zero–temperature quantum phase transition. We present numerical results demonstrating that at this transition the system changes from being quasi-integrable to quantum chaotic. By deriving an exact solution in the thermodynamic limit we relate this phenomenon to a localisation–delocalisation transition in which a macroscopic superposition is generated. We also describe the classical analogues of this behaviour.

At zero temperature, systems of N interacting particles can exhibit a quantum phase transition (QPT) as a function of a coupling parameter λ in the limit that $N \rightarrow \infty$. How do the precursors of such a transition influence quantum chaotic (and non-chaotic) behaviour of the same system for finite N ?

One of the most direct indicators of the emergence of quantum chaos is the change in energy level spacing statistics from Poissonian to being described by the Gaussian ensembles of Random Matrix Theory. Although this change-over has been observed in many systems [1, 2, 3, 4], only in a comparatively few, isolated cases has the onset of quantum chaos been correlated with the presence of a QPT. Important examples include spin glass shards, which have recently been used in modeling the onset of chaos in quantum computers [5], the Lipkin model [6], the interacting boson model [7], and the three–dimensional Anderson model [8, 9], where the change in level statistics occurs at the metal–insulator (localisation–delocalisation) transition found in disordered electronic systems.

In this Letter we consider the Dicke Hamiltonian (DH) [10], a quantum-optical model describing the interaction of N two-level atoms with a number of bosonic modes. We demonstrate that a crossover between Poisson and Wigner–Dyson statistics in this model for finite N is intimately connected to a mean-field type superradiance QPT.

The simplicity and generality of the Dicke Hamiltonian have afforded it appeal both for the investigation of quantum chaos, and as a model for phase transitions at a critical coupling λ_c induced by the interaction with light. The level statistics for finite N have revealed the existence of quantum chaos in certain isolated regimes of the model [11, 12]. On the other hand, the QPT aspect for $N \rightarrow \infty$ has been discussed in the context of superradiance [13, 14], and recently for exciton condensation [15]. Here, we derive an *exact* solution for all eigenstates, eigenvalues and critical exponents in the thermodynamic limit, and show that above the critical point $\lambda = \lambda_c$ the ground-state wavefunction bifurcates into a macroscopic superposition for any $N < \infty$. Our numerical results indicate that a localisation–delocalisation transition for

$N \rightarrow \infty$ underlies the cross-over between Poissonian and Wigner level–spacing distributions for finite N . Furthermore, we use an exact Holstein–Primakoff transformation to derive the classical limit of the model for arbitrary N and find a transition at $\lambda = \lambda_c$ from regular to chaotic trajectories. The latter are delocalised around *two* fixed points in phase space which we conjecture constitute the classical analogue of the macroscopic superposition. The emergence of this state in the Dicke model is related to a conserved parity which becomes spontaneously broken in the thermodynamic limit.

We consider the single–mode Dicke Hamiltonian (DH)

$$H = \omega_0 J_z + \omega a^\dagger a + \frac{\lambda}{\sqrt{2j}} (a^\dagger + a) (J_+ + J_-), \quad (1)$$

where J_z , J_\pm are the usual angular momentum operators for a pseudo–spin of length $j = N/2$, and a , a^\dagger are the bosonic operators of the field. The atomic level–splitting is given by ω_0 , ω is the field frequency, and λ is the atom–field coupling. Crucially, we have not made the rotating–wave approximation (RWA), as this would render the model integrable and destroy the phenomena that we describe here [12]. There is a conserved parity Π associated with the DH, which is given by $\Pi = \exp \{i\pi [a^\dagger a + J_z + j]\}$, such that $[H, \Pi] = 0$. The eigenvalues of Π are ± 1 and, unless stated, we shall work exclusively in the positive parity subspace.

We begin by discussing the properties of the system in the thermodynamic limit $N, j \rightarrow \infty$. In this limit the system becomes integrable for all λ , and we can derive effective Hamiltonians to describe the system exactly in each of its two phases. We employ a procedure similar to Hillery and Mlodinow’s analysis of the RWA Hamiltonian [16], and introduce the Holstein–Primakoff representation of the angular momentum operators, $J_+ = b^\dagger \sqrt{2j - b^\dagger b}$, $J_- = \sqrt{2j - b^\dagger b} b$, $J_z = (b^\dagger b - j)$, where b and b^\dagger are bosonic operators [17]. Making these substitutions allows us to write the DH as a two-mode Hamiltonian. Below the phase transition, we proceed to the thermodynamic limit by expanding the square roots and neglecting terms with powers of j in the denominator. This yields the effective Hamiltonian $H^{(1)} = \omega_0 b^\dagger b + \omega a^\dagger a + \lambda (a^\dagger + a) (b^\dagger + b) - j\omega_0$. This

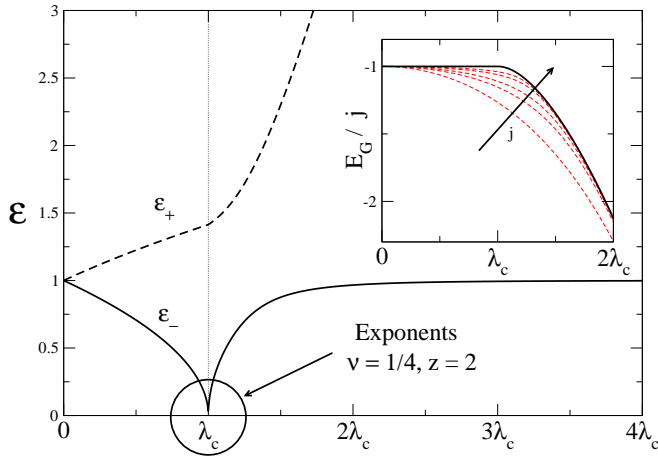


FIG. 1: Excitation energies ε_{\pm} of the DH in the thermodynamic limit. Inset: scaled ground-state energy, E_G/j , in the thermodynamic limit (solid line) and at various finite values of $j = 1/2, 1, 3/2, 3, 5$ (dashed lines). The Hamiltonian is on scaled resonance $\omega = \omega_0 = 1$.

bi-linear Hamiltonian may then be diagonalised to give $H^{(1)} = \varepsilon_-^{(1)} c_-^\dagger c_- + \varepsilon_+^{(1)} c_+^\dagger c_+ - j\omega_0$, where $\varepsilon_{\pm}^{(1)}$ are the excitation energies of the low-coupling phase, and are given by

$$2 \left(\varepsilon_{\pm}^{(1)} \right)^2 = \omega^2 + \omega_0^2 \pm \sqrt{(\omega_0^2 - \omega^2)^2 + 16\lambda^2 \omega \omega_0}. \quad (2)$$

The energy $\varepsilon_-^{(1)}$ is real only for $\lambda \leq \sqrt{\omega\omega_0}/2 = \lambda_c$, which locates the phase transition. We derive an effective Hamiltonian above λ_c by first displacing each oscillator mode in the Holstein-Primakoff DH by a quantity proportional to \sqrt{j} , and then neglecting terms as above. With an appropriate choice of displacements, this process also yields a bi-linear Hamiltonian, which may be diagonalised to a form similar to $H^{(1)}$, but with different vacuum and excitation energies, the latter of which are given by

$$2\lambda_c^4 \left(\varepsilon_{\pm}^{(2)} \right)^2 = \omega_0^2 \lambda^4 + \omega^2 \lambda_c^4 \pm \sqrt{(\omega_0^2 \lambda^4 - \omega^2 \lambda_c^4)^2 + 4\omega^2 \omega_0^2 \lambda_c^8}. \quad (3)$$

The excitation energy $\varepsilon_-^{(2)}$ of this second Hamiltonian $H^{(2)}$ is real only above the phase transition. There are two independent choices of displacements, each of which yield a different effective Hamiltonian above λ_c . This is a consequence of the fact that at the QPT the Π symmetry is spontaneously broken.

In Fig. 1 we plot as a function of coupling the behaviour of the excitation energies and the ground-state energy, which is itself continuous but possesses a discontinuity in its second derivative at λ_c . Below the phase transition the ground-state is composed of an empty field with all the atoms unexcited and hence $\langle J_z \rangle_G/j = -1$

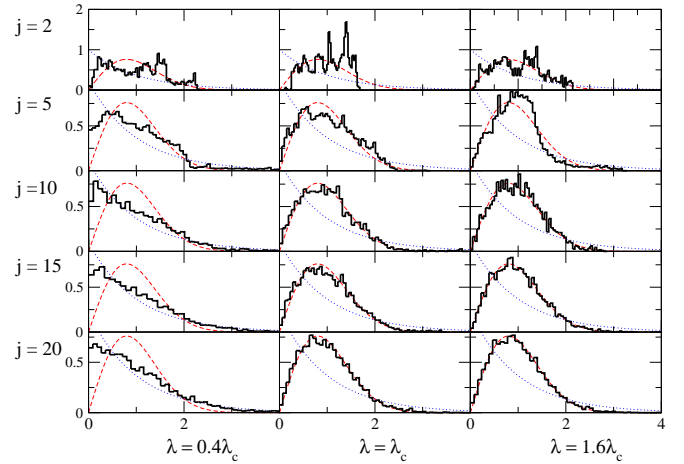


FIG. 2: Plots of nearest-neighbour distributions $P(S)$ for the Dicke Hamiltonian, for different couplings λ and pseudo-spin j . Also plotted are the universal Poissonian (dots) to Wigner (dashes) distributions.

and $\langle a^\dagger a \rangle_G/j = 0$. Above λ_c , the field is macroscopically occupied, $\langle a^\dagger a \rangle_G/j = 2(\lambda^4 - \lambda_c^4)/(\omega\lambda)^2$, and the atoms acquire a macroscopic inversion, $\langle J_z \rangle_G/j = -\lambda_c^2/\lambda^2$. At the phase transition, the excitation energy ε_- vanishes as $|\lambda - \lambda_c|^{z\nu}$ and the characteristic length scale $l_- = 1/\sqrt{\varepsilon_-}$ diverges as $|\lambda - \lambda_c|^{-\nu}$, with exponents given by $\nu = 1/4$, $z = 2$ on resonance.

To investigate the level statistics of the system, we numerically diagonalise the Hamiltonian in the basis $\{|n\rangle \otimes |j, m\rangle\}$, where $a^\dagger a|n\rangle = n|n\rangle$, and $|j, m\rangle$ are the Dicke states, $J_z|j, m\rangle = (b^\dagger b - j)|j, m\rangle = m|j, m\rangle$. We restrict ourselves to the positive parity subspace by considering only states with $n + m + j$ even. We then unfold the resulting energy spectrum to rid it of secular variation, form the level spacings $S_n = E_{n+1} - E_n$, and then construct the nearest-neighbour distribution function $P(S)$. Finally, we normalise the results for comparison with the universal ensembles of Random Matrix Theory. In the following, we shall use the term ‘‘quasi-integrable’’ to denote systems exhibiting Poissonian level statistics, and reserve ‘‘integrable’’ for systems possessing exact solutions.

Figure 2 shows the $P(S)$ distributions obtained for the DH at various values of the coupling, and for various values of j . At low j the $P(S)$ clearly do not correspond to any of the universal ensembles. This is most keenly observed in the $j = 1/2$ case (identical to the Rabi Hamiltonian [18]), where the spectrum is of ‘‘picket-fence’’ character [19], characteristic of one-dimensional systems or harmonic oscillators [20]. For couplings less than the critical value, $\lambda < \lambda_c$, we see that as we increase j , the $P(S)$ approaches ever closer the Poissonian distribution, $P_P(S) = \exp(-S)$. At and above λ_c the spectrum is seen to converge onto the Wigner distribution $P_W(S) = \pi S/2 \exp(-\pi S^2/4)$, characteristic of quantum

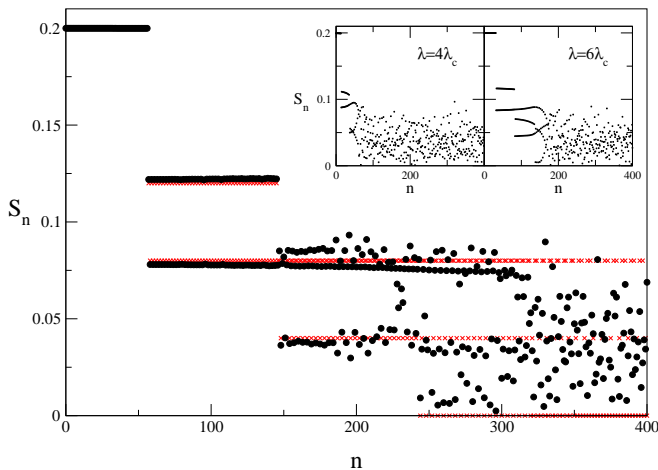


FIG. 3: Nearest-neighbour spacing $S_n = E_{n+1} - E_n$ vs. eigenvalue number n plot for $j = 5$ with $\lambda = 8\lambda_c$. Horizontal crosses: results for the integrable $\lambda \rightarrow \infty$ Hamiltonian. Inset: $j = 5$ results with $\lambda = 4\lambda_c$ and $\lambda = 6\lambda_c$.

chaos. This demonstrates that the precursors of the QPT in this model lead to a cross-over from quasi-integrable to quantum chaotic behaviour at $\lambda \approx \lambda_c$.

A further transition between integrable and chaotic behaviour is observed in the sequence of level spacings S_n . The $\lambda \rightarrow \infty$ limit of the Hamiltonian is integrable for arbitrary j , having eigen-energies $E_{nm} = \frac{\omega}{j}n - \frac{2\lambda^2}{\omega j^2}m^2$, where $n = 0, 1, 2, \dots$ and $m = -j, \dots, +j$. As λ is increased from λ_c to approach this limit with j fixed, the spectrum reverts from Wigner-like to integrable. However, it does not follow the usual transition sequence, but rather through a sequence illustrated by Fig. 3. The spectrum becomes very regular at low energy, where it approximates the integrable $\lambda \rightarrow \infty$ results closely. Outside the regular region the spectrum is well described by the Wigner surmise, and the energy-scale over which the change between the two regimes occurs is seen to be surprisingly narrow. As coupling is increased, the size of the low-energy integrable window increases, until it eventually engulfs the whole spectrum as $\lambda \rightarrow \infty$.

We now proceed to consider the wavefunctions of the system by introducing an abstract position-momentum representation for each of the boson modes via $x \equiv \frac{1}{\sqrt{2\omega}}(a^\dagger + a)$; $p_x \equiv i\sqrt{\frac{\omega}{2}}(a^\dagger - a)$, and $y \equiv \frac{1}{\sqrt{2\omega_0}}(b^\dagger + b)$; $p_y \equiv i\sqrt{\frac{\omega_0}{2}}(b^\dagger - b)$. In this representation the action of the parity operator Π corresponds to rotation by π about the origin. The ground state of the system on scaled resonance for $j = 5$ is plotted for different couplings in Fig. 4. These wavefunctions were obtained by diagonalising the Hamiltonian in the same basis as was used to calculate $P(S)$ and representing the basis vectors $|n\rangle \otimes |m, j\rangle$ by products of harmonic oscillator eigenfunctions. For the non-interacting system ($\lambda = 0$), the wavefunction is a product of two indepen-

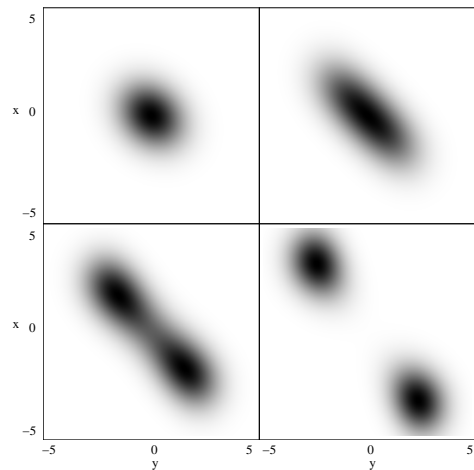


FIG. 4: The modulus of the ground-state wavefunction $\psi(x, y)$ of the Dicke Hamiltonian in the abstract x - y representation for finite $j = 5$, at couplings of $\lambda/\lambda_c = 0.4, 1.0, 1.2, 1.4$. Black corresponds to $\text{Max}|\psi|$ and white corresponds to zero.

dent Gaussians. As the coupling increases, the two modes start mixing, leading to a stretching of the single-peaked wavefunction. Around the critical coupling ($\lambda \approx \lambda_c$), the wavefunction bifurcates to become a double-peaked function, and with further increases in coupling the two lobes at $(\pm x_0, \mp y_0)$ move away from each other in their respective quadrants of the $x - y$ plane. Since x_0 and y_0 are of the order of \sqrt{j} , for large j the ground state evolves into a superposition of two macroscopically distinguishable parts, which may be considered as a ‘‘Schrödinger’s cat’’. The formation of this state constitutes a delocalisation of the ground-state wavefunction, which is also observed in the excited states. This localisation-delocalisation transition is consistent with the transition between Poisson and Wigner distributions in the spectrum [21]. The suppression of chaos at low j is then seen to be due to the fact that for low j only a few excitations are permitted in the b -mode. This restricts the extent of the wavefunction in the y -direction, inhibiting delocalisation, and yielding the non-generic $P(S)$ seen in Fig. 2. It should be noted that an actual spontaneous symmetry-breaking transition occurs above λ_c in the $j \rightarrow \infty$ limit which removes the two lobes so far from one another that they cease to overlap and thus can be considered independently. This breaks the Π symmetry of the model, allowing us to obtain the earlier exact results by using an effective Hamiltonian for each lobe. These Hamiltonians are identical in form, have identical spectra, thus demonstrating that in the thermodynamic limit, each energy level in the high-coupling phase is doubly degenerate and the macroscopic superposition is broken in half.

Finally, this position representation allows us to study the classical analogues of this QPT and the accompanying onset of chaos in a very natural way. By setting

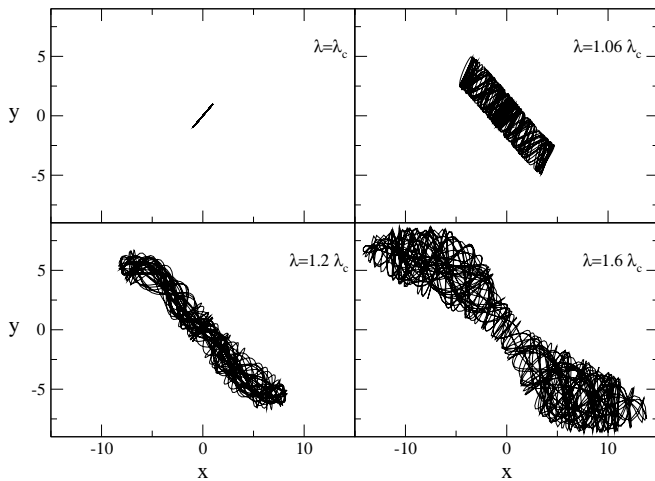


FIG. 5: Typical classical phase space projections ($p_x = p_y = 0$) for the classical Dicke Hamiltonian of Eq. (4) with $\lambda/\lambda_c = 1.0, 1.06, 1.2, 1.6$, for $j = 30.0$, $\omega = \omega_0 = 1$. Initial conditions were $x(0) = y(0) = 1$, $p_x(0) = p_y(0) = 0$. The abrupt change to complex motion is observed above $\lambda = \lambda_c$.

the commutators $[x, p_x]$ and $[y, p_y]$ to zero, the classical Hamiltonian corresponding to Eq. (1) is seen to be

$$H_{cl} = -j\omega_0 + \frac{1}{2}(\omega_0^2 y^2 + p_y^2 + \omega^2 x^2 + p_x^2 - \omega - \omega_0) + 2\lambda\sqrt{\omega\omega_0}xy\sqrt{1 - \frac{1}{4\omega_0 j}(\omega_0^2 y^2 + p_y^2 - \omega_0)}. \quad (4)$$

Space limitations here only allow us to point out two significant features. Firstly, below λ_c there is only one fixed point of the flow, namely $x = y = p_x = p_y = 0$. At $\lambda = \lambda_c$ this situation changes abruptly and two new fixed points appear at $(x, y) = (\pm x_{cl}, \mp y_{cl})$ with $p_x = p_y = 0$, where x_{cl} and y_{cl} are approximately equal to the centres of the wavefunction lobes x_0, y_0 for large j . Secondly, parametric plots of typical trajectories obtained from Eq. (4) (Fig. 5) demonstrate that the system undergoes a rapid change at $\lambda = \lambda_c$ from a very simple quasi-periodic motion to intricate chaotic behaviour, in agreement with the results of the quantum model. Note that the correspondence between this classical system and the original quantum one is significantly greater than previous semi-classical treatments [22], and that this holds for any j , not just for $j \rightarrow \infty$.

We mention that larger system sizes are required to check if there exists a critical level statistics of our model at λ_c [9], and that an examination of the exceptional points [6] of this model may yield further insight. Future work also includes a study of related models to determine the generality of the features described here.

In summary, we have seen that the $P(S)$ distribution of the DH at finite N changes from being Poissonian to Wigner at approximately λ_c , indicating the emergence of quantum chaos. The ground-state wavefunction bifurcates at this point, forming a macroscopic superposition.

The underlying quantum phase transition is reflected in the classical model derived here by the appearance of two new fixed points at λ_c , where a transition between regular and chaotic trajectories occurs.

This work was supported by projects EPSRC GR44690/01, DFG Br1528/4-1, the WE Heraeus foundation and the UK Quantum Circuits Network.

* emary@theory.phy.umist.ac.uk

- [1] T. Guhr, A. Müller-Groeling, and H. A. Weidenmüller, Phys. Rep. **299**, 189 (1998); F. Haake, *Quantum Signatures of Chaos*, (Springer, Berlin, 2001).
- [2] O. Bohigas, M. J. Giannoni, and C. Schmidt, Phys. Rev. Lett. **52**, 1 (1984).
- [3] D. Delande and J. C. Gay, Phys. Rev. Lett. **57**, 2006 (1986).
- [4] Ph. Jacquod and D. L. Shepelyansky, Phys. Rev. Lett. **79**, 1837 (1997).
- [5] B. Georgeot and D. L. Shepelyansky, Phys. Rev. Lett. **81**, 5129 (1998); Phys. Rev. E **62**, 3504 (2000).
- [6] W. D. Heiss and A. L. Sannino, Phys. Rev. A **43**, 4159 (1991); W. D. Heiss and M. Müller, Phys. Rev. E **66**, 016217 (2002).
- [7] Y. Alhassid and N. Whelan, Nucl. Phys. A **556** 42 (1993); P. Cejnar and J. Jolie, Phys. Rev. E **58**, 387 (1998).
- [8] For a review, see P. A. Lee and T. V. Ramakrishnan, Rev. Mod. Phys. **57**, 287 (1985).
- [9] I. K. Zharekeshev and B. Kramer, Phys. Rev. B **51**, 17239 (1995); Phys. Rev. Lett. **79**, 717 (1997).
- [10] R. H. Dicke, Phys. Rev. **93**, 99 (1954).
- [11] R. Graham and M. Höhnert, Phys. Rev. Lett. **57**, 1378 (1986).
- [12] C. H. Lewenkopf, M. C. Nemes, V. Marvulle, M. P. Pato, and W. F. Wrenszinski, Phys. Lett. A **155**, 113 (1991).
- [13] K. Hepp and E. H. Lieb Ann. Phys. NY **76**, 360 (1973); Y. K. Wang and F. T. Hioe, Phys. Rev. A **7**, 831 (1973).
- [14] A. V. Andreev, V. J. Emel'yanov, and Yu. A. Il'inskii, *Cooperative Effects in Optics*, (IOP Publishing, Bristol, 1993); M. G. Benedict *et al.*, *Super-Radiance*, (IOP Publishing, Bristol, 1996).
- [15] P. R. Eastham and P. B. Littlewood, Phys. Rev. B **64**, 235101 (2001).
- [16] M. Hillery and L. D. Mlodinow, Phys. Rev. A **31**, 797 (1984).
- [17] T. Holstein and H. Primakoff, Phys. Rev. **58**, 1098 (1949).
- [18] I. I. Rabi, Phys. Rev. **51**, 652 (1937); R. F. Bishop and C. Emary, J. Phys. A **34**, 5635 (2001).
- [19] M. Kus, Phys. Rev. Lett. **54**, 1343 (1985).
- [20] M. V. Berry and M. Tabor, Proc. R. Soc. Lond. A **356**, 375 (1977).
- [21] S. Fishman, D. R. Grempel, R. E. Prange, Phys. Rev. Lett. **49**, 509 (1982); Phys. Rev. A **29**, 1639 (1984); R. E. Prange in *Quantum Chaos*, ed. H. A. Cerdeira, R. Ramaswamy, M. C. Gutzwiller, G. Casati (World Scientific, 1991).
- [22] P. W. Milonni, J. R. Ackerhalt, and H. W. Galbraith, Phys. Rev. Lett. **50**, 966 (1983); R. Graham and M. Höhnert, Z. Phys. B **57**, 233 (1984).